Journal of Materials Chemistry A

Control Synthesis of Hierarchical ZSM–5 for Catalytic Fast Pyrolysis of Cellulose to Aromatics

Journal:	*Journal of Materials Chemistry A*
Manuscript ID	TA-ART-09-2018-008930
Article Type:	Paper
Date Submitted by the Author:	13-Sep-2018

Complete List of Authors:
Chen, Hao; Zhejiang University,
Shi, Xu; Zhejiang University
Liu, Jianfang; Lawrence Berkeley National Laboratory
Jie, Kecheng; The University of Tennessee, Department of Chemistry
Zhang, Zihao; Zhejiang University,
Hu, Xiaobing; Brookhaven National Laboratory
Zhu, Yimei; Brookhaven National Laboratory,
Lu, Xiuyang; Zhejiang University, Chemical and Biological Engineering
Fu, Jie; Zhejiang University, Department of Chemical and Biological Engineering
Huang, He; Nanjing Tech University,
Dai, Sheng; Oak Ridge National Laboratory,

Journal Name

ARTICLE

Control Synthesis of Hierarchical ZSM–5 for Catalytic Fast Pyrolysis of Cellulose to Aromatics

Received 00th January 20xx,
Accepted 00th January 20xx

DOI: 10.1039/x0xx00000x

www.rsc.org/

Hao Chen[a, b], Xu Shi[a, d], Jianfang Liu[e], Kecheng Jie[b], Zihao Zhang[a], Xiaobing Hu[f], Yimei Zhu[f], Xiuyang Lu[a], Jie Fu[*a], He Huang[*a, d], Sheng Dai[*b, c]

Zeolite materials play a significant role throughout the oil refining and petrochemical industry. The microporous ZSM-5 with high degree of crystallinity but low mass transfer, while hierarchical ZSM-5 showed low degree of crystallinity as well as the acidity. In this work, we first report the synthesis of ZSM–5 with a new morphological structure, which has nanocrystalline ZSM–5 particles on the surface of an intact ZSM–5 zeolite not only improved the mass transfer of microporosity but also overcame the disadvantage of hierarchical ZSM-5 that low degree of crystallinity and acidity. This new and very efficient structure with both intracrystal microporosity and intercrystal macroporosity, formed by secondary crystallization after the intact ZSM–5 zeolite was synthesized, was demonstrated by transmission electronic microscopy, N_2 adsorption and desorption and X–ray diffraction. The obtained ZSM–5 zeolite showed a uniform size (~200 nm), high crystallinity acidity, and a suitable hierarchical structure that exhibited excellent properties in the catalytic fast pyrolysis of cellulose to produce aromatics.

Introduction

Traditionally, more than 85% of the production of aromatic chemicals depends primarily on the catalytic reforming of petroleum resources [1–3]. Thus, the ability to produce aromatics from renewable and environmentally friendly resources is highly desirable to ease pressures on petroleum supplies and the environment. Catalytic fast pyrolysis (CFP) is a promising technology for the direct conversion of biomass, such as cellulose and lignin, into valuable aromatics [4–6]. It has attracted considerable attention because of its use of alternative sources, renewability, and reuse of CO_2 [7].

Crystalline porous materials (zeolites, ordered mesoporous silica, and metal–organic frameworks) are important in many catalytic reactions with high scientific and industrial impact [8–11]. The zeolite HZSM–5 was reported to be an efficient catalyst for producing aromatic hydrocarbons from biomass because ZSM–5 has a three–dimensional [3D] microporous system with average pore dimensions of 5.5–5.6 Å, similar to the kinetic diameters of benzene, toluene, p–xylene, indene, furfural, and 2–methyl furan [12, 13]. However, ZSM–5 is limited by low mass–transfer rates of large reactants and products during pyrolysis [14, 15]. Recently, considerable attention has been paid to hierarchical materials [16, 17] in catalysis applications. Groen and Pérez–Ramírez made very significant contributions in the development of hierarchical zeolites obtained by alkali and acid treatments [18–20]. Hierarchical ZSM–5 was also reported to have a positive effect on the CFP of cellulose to produce aromatics [21–23].

The synthesis of zeolite materials with tailored structures for desired functions is very important for designated reactions, but it remains a significant challenge [24-26]. Fickel et al. [27] reported the copper-exchanged small-pore zeolites (Cu-SSZ-13, Cu-SSZ-16, and Cu-SAPO-34) and display superior selective catalytic reduction. Ryoo et al. [28, 29] designed bifunctional surfactants for the formation of zeolites with both mesoporous and microporous length scales simultaneously, yielding MFI zeolites with tunable mesoporosity. Zhao et al. designed many functional zeolites, such as an HZSM–5@SBA–15 core–shell zeolite [30] and nanorod–aggregated ZSM–5 microspheres [29]. Hierarchical ZSM–5 prepared by organosilane modification was reported to have nanoscale ZSM–5 particles that had much larger external surface areas, shorter diffusion path lengths, and more accessible active sites than conventional zeolites and delivered excellent catalytic performance for a variety of reactions [24, 31, 32]. Although it was reported the synthesis of hierarchical ZSM-5 using sucrose as hard template, which showed high activity for CFP of cellulose[33], this work only used one kind of template, sucrose, to form suitable mesoporous structure in ZSM-5 without any morphological and mesopores controlling[33]. Thus, a suitable zeolite structure designed via organosilane–modification to enhance the catalytic activity in

[a.] Key Laboratory of Biomass Chemical Engineering of Ministry of Education, College of Chemical and Biological Engineering, Zhejiang University, Hangzhou 310027, China.
[b.] Department of Chemistry, The University of Tennessee, Knoxville, TN, USA.
[c.] Oak Ridge National Laboratory, Oak Ridge, TN, USA.
[d.] School of Pharmaceutical Sciences, Nanjing Tech University, Nanjing 211800, China.
[e.] The Molecular Foundry, Lawrence Berkeley National Laboratory, Berkeley CA 94720, USA
[f.] Condensed Matter Physics and Material Science Department, Brookhaven National Laboratory, Upton, New York 11973, USA
Electronic Supplementary Information (ESI) available: [details of any supplementary information available should be included here]. See DOI: 10.1039/x0xx00000x

CFP of cellulose to produce aromatics has great prospects for application.

In this work, hierarchical nanocrystalline ZSM–5 was synthesized by hydrothermal crystallization using four organosilanes with different carbon chain lengths, trimethoxymethylsilane (MTS), trimethoxy(propyl)silane (PTS), trimethoxy(octyl)silane (OTS), and hexadecyltrimethoxysilane (HTS), as mesoporous templates. We first reported the synthesis of a new ZSM–5 structure that contained nanocrystalline ZSM–5 particles on the surface of an intact ZSM–5 zeolite, using HTS as a mesoporous template. The new structure, with regular pore formation and acidity affected by the carbon chain length of the organosilane, was demonstrated by transmission electronic microscopy (TEM), N_2 adsorption and desorption (N_2–BET), X–ray diffraction (XRD) and temperature programmed desorption of NH_3 (NH_3–TPD). The CFP of cellulose to produce aromatics in a microreactor system was investigated to study the influence of mesoporous templates in controlling the shape and hierarchical structure, which affected the yield and selectivity of the aromatics.

Results and discussion

Catalyst characterization

The XRD patterns of four HZSM–5 zeolites prepared using different organosilanes are shown in **Figure 1**. All the samples show the same characteristic peaks in the range of 7–9° and 22.5–25.0°, which were attributed to the morphology of the ZSM–5 zeolite [34, 35]. The relative crystallinity was determined based on the intensity of the characteristic peaks in the range between 6–9° and 22.5–25.0°. The intensity of the peaks was much higher for ZSM–5 synthesized by HTS (donated as ZHTS) than for ZSM–5 synthesized by MTS (donated as ZMTS), PTS, (donated as ZPTS) and OTS (donated as ZOTS); this finding means that ZHTS had a higher relative crystallinity.

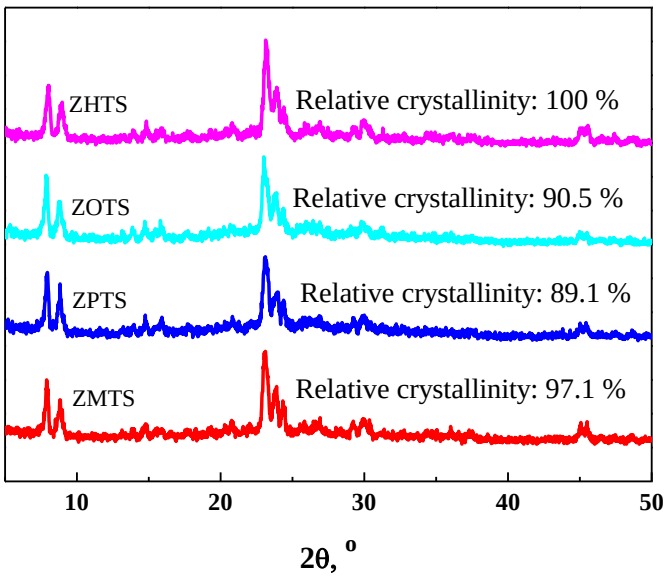

Figure 1. XRD patterns of hierarchical HZSM–5 zeolites synthesized using trimethoxymethylsilane (MTS), trimethoxy(propyl)silane (PTS), trimethoxy(octyl)silane (OTS) and hexadecyltrimethoxysilane (HTS) under pre–crystallizing 12 h.

The TEM results, which proved the structure of the synthesized hierarchical HZSM–5 zeolites, are shown in **Figure 2**. It was observed clearly that there is no aggregated structure for ZMTS, and the each particle existed separately. The size of each ZMTS particle was uniform at 200 nm. The micropores in ZMTS are seen clearly as shown in **Figure 2c** at about 0.52 nm. The ZPTS and ZOTS samples showed obvious microspheres composed of many nanosize ZSM–5 particles **(Figure 2 d–i)**, meaning that the carbon chain lengths of PTS and OTS were suitable to synthesize nanosized ZSM–5 particles and form microspherical structures. Interestingly, the ZHTS exhibited a different ZSM–5 structure that has not been reported before, as shown in **Figure 2 j–l**. The samples synthesized using HTS showed a new structure with some small nanocrystalline ZSM–5 particles grafted on the surface of an intact ZSM–5 zeolite, which made the ZSM-5 with intracrystal micropores and large intercrystal mesopores. All the samples were in a uniform size range of around 200 nm, as shown in **Figure 2 j**. These nanocrystalline ZSM–5 particles were formed by secondary crystallization after the intact ZSM–5 zeolite was synthesized in the same manner as ZMTS. Note that TEM detected the classic micropores of ZSM–5 at about 0.52 nm for all the samples, as shown in **Figure 2 c, f, i and l**. The micropores detected by TEM not only were centered at 0.52 nm but also had an equilateral polygon shape because the ZSM–5 pores were reported to be 10–member ring pores. **Figure 3** shows the TEM images with different shooting angles of synthesized hierarchical ZSM–5, which proved this new structure more clearly. This structure solved the disadvantage of the low crystallinity and acidity of hierarchical ZSM-5 nano microspheres and kept the high mass transfer ability.

As shown in the Figure S4, the ZMTS showed “classic-boat” microporous structure while ZOTS and ZPTS showed microspheres with micropores and intercrystal mesopores. Meanwhile, the ZHTS showed the structure with nanocrystalline ZSM–5 particles on the surface of an intact ZSM–5 zeolite. The results were in accord with the results obtained from TEM.

Journal Name

ARTICLE

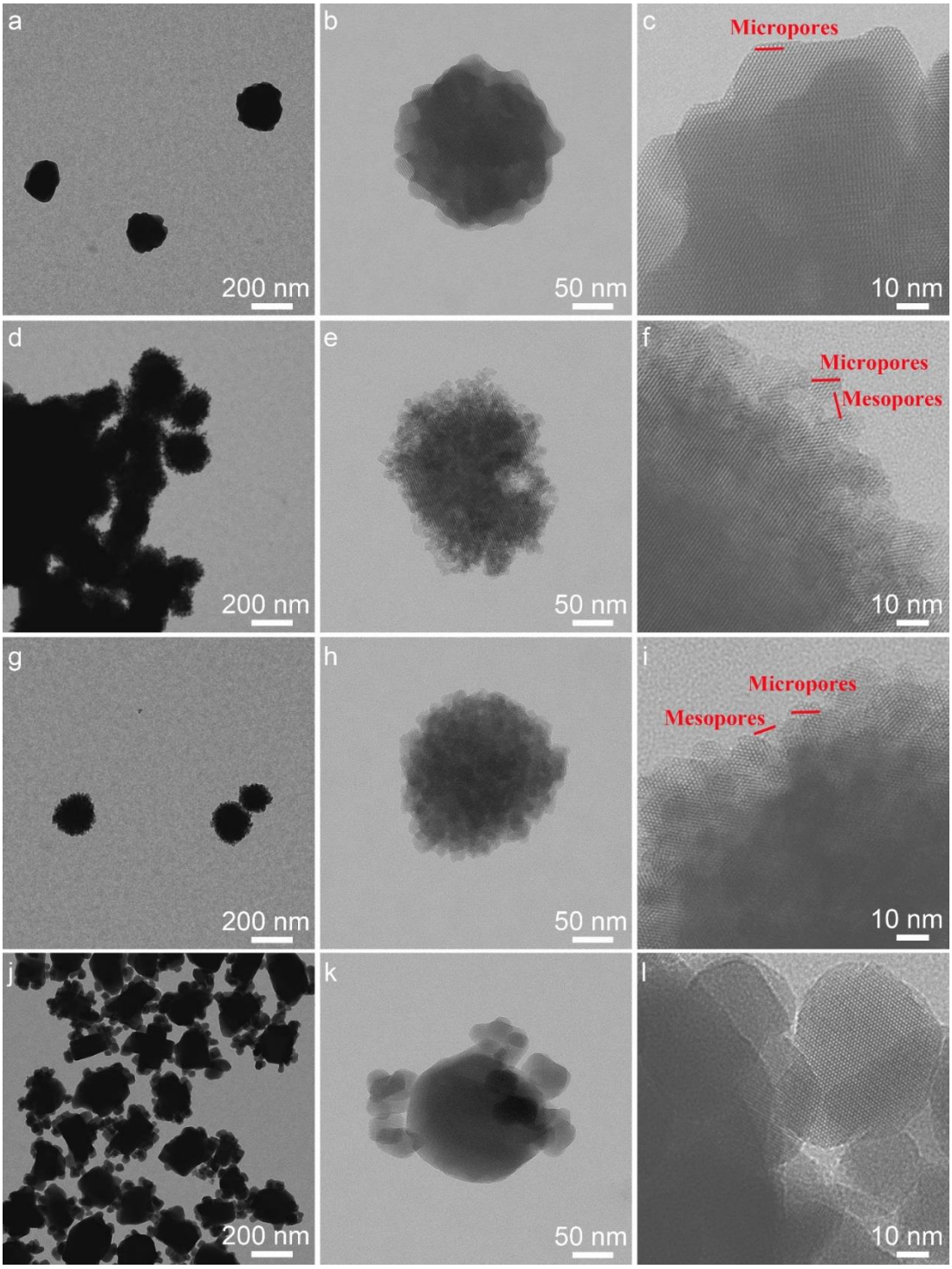

Figure 2. TEM images of hierarchical HZSM–5 zeolites synthesized using [a–c] trimethoxymethylsilane (MTS); [d–f] trimethoxy[propyl]silane (PTS); [g–i] trimethoxy[octyl]silane (OTS), and [j–l] hexadecyltrimethoxysilane (HTS) under pre–crystallizing for 12 h.

Journal Name

ARTICLE

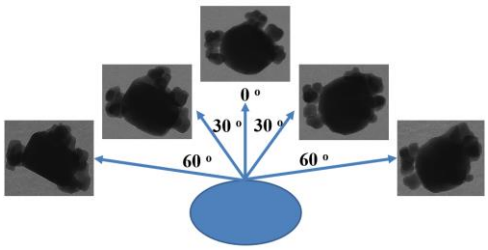

Figure 3. TEM images with different shooting angles of hierarchical ZSM–5 synthesized using hexadecyltrimethoxysilane (HTS) under pre–crystallizing 12 h.

The carbon chain lengths of the organosilanes influenced the growth of ZSM–5 significantly. The HTS had the longest carbon chains among the four organosilanes and produced ZSM–5 particles with a very interesting structure: several nanocrystalline ZSM–5 particles grew on the surface of an intact ZSM–5 zeolite. This meant that secondary crystallization occurred on the surfaces of ZSM–5 particles produced in the first crystallization step. The structure with a large ZSM–5 particle and several smaller particles indicates that the main carbon chains of the HTS entered the body of the ZSM–5. They formed intact ZSM–5 particles, and part of the HTS was exposed on the surfaces of the particles. Then the exposed portions of the HTS acted as a silicon source and formed the small ZSM–5 particles. The effects of the carbon chain lengths of the organosilanes on the growth of ZSM–5 are proposed as shown in **Scheme 1**. However, the carbon chain in MTS was very short, and the chains served only as a silicon source during the synthesis procedure. The pores in ZMTS were all typical micropores and same with conversional ZSM–5 (donated as HZ–Con) (see **Figure 2**). For PTS and OTS, the carbon chains of the two organosilanes were longer than in MTS, and they acted not only as a silicon source but also as a template for the mesopores. The ZSM–5 prepared using an organosilane modification approach attracted great attention and was reported to produce nanoscale ZSM–5 particles [36, 37]. Thus, PTS and OTS were suitable for synthesizing aggregated hierarchical ZSM–5 microspheres composed of small ZSM–5 granules.

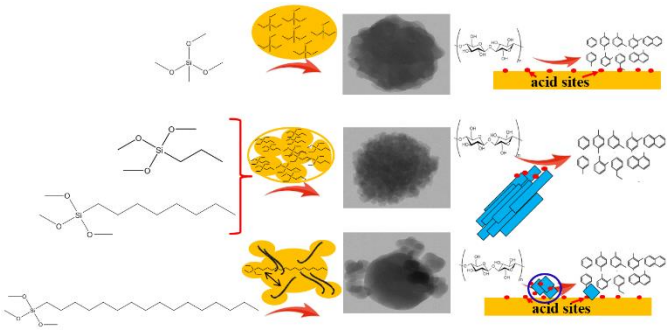

Scheme 1. Schematic illustration of the formation of ZSM–5 with different structures during crystallization, using organosilanes with different carbon chain lengths.

It was accepted that the growth of the MFI zeolite contained two steps: nucleation and crystal growth [38]; and its growth mechanism was juxtaposed between classical models (two–dimensional [2D] layer growth) that postulate silica molecules as primary growth units, and nonclassical pathways ([3D] island growth) based on the aggregation of metastable silica nanoparticle precursors [39]. Based on the results of the TEM characterization, we proposed an evolution mechanism for ZSM–5 with a controllable hierarchical structure. Here, with the presence of MTS, the conventional mechanisms involved 2D layer nucleation and spreading to form a well–defined faceted crystal structure (HZ–Con) for the growth of ZMTS. During the crystallization using PTS and OTS, the PTS and OTS had an affinity potential towards aluminosilicate and silica precursors because of the suitable carbon chain length like the reported work[38]. The crystal growth was proceeded by a nonclassical 3D island growth mechanism involving the direct attachment of nanoparticles, yielding microspheres as shown in **Figure 2** [38]. But for HTS as template, the carbon chain length was long enough to make it prone to adsorb more aluminosilicate precursors in the tail end, which restrained the formation of alunimsilicates nanoparticles. Therefore, the molecular addition became the predominant mechanism involving 2D layer nucleation and stepwise advancement of layers, which produced faceted ZSM-5 crystals. Then, the more aluminosilicate precursors adsorbed in the tail end of HTS gave the another 2D layer, then small particles continued to grow one by one via a second 2D layer growth pathway to form the new structure. We also added the experiment using trimethoxyoctadecylsilane (TTS), which have two carbons longer carbon chain than HTS, to see whether the zeolites with structures similar to that of ZHTS can be obtained. The results showed that the same structure that nanocrystalline ZSM–5 particles grew on the surface of an intact ZSM–5 zeolite.

The N_2–BET isotherms and pore size distributions for hierarchical nanocrystalline HZSM–5 prepared with different organosilanes are illustrated in **Figure 4**. The N_2–BET isotherms of

ZMTS and ZHTS present type I isotherms with the plateaus starting at a very low relative pressure, which implies that the parent zeolite was dominated by the microporous structure. The intercrystal mesopores in ZHTS were too large to be detected by N_2–BET, which should be called intercrystal macropores and determined by and mercury injection (**Figure S2**). For PTS and OTS templates, it was found that the N_2 adsorption isotherm contains a steep uptake below $P/P_0 = 0.02$ and a hysteresis loop from $P/P_0 = 0.45$ to about $P/P_0 = 1$, and the ZSM-5 was composed of small ZSM-5 particles forming the nanoparticle-aggregated ZSM-5 microspheres from TEM images. Thus, the mesopores detected by N_2-BET ascribed to the agglomeration of nanoparticles (intercrystal mesopores) [24]. Based on the results of the pore size distribution, it was found that HTS did not produce any mesopores in the framework of hierarchical ZSM–5 due to the intercrystal pores between each particle was too large (intercrystal macropores) to be detected in N_2-BET.

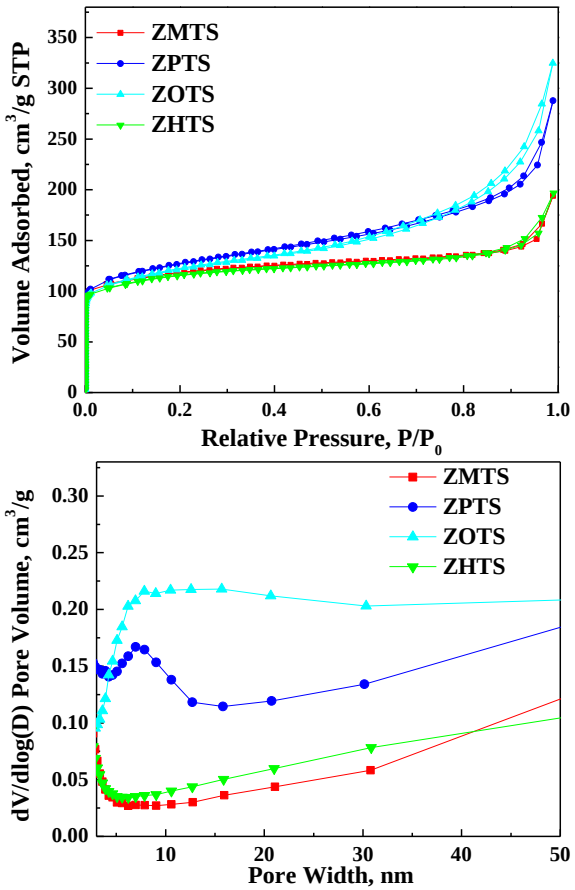

Figure 4. N_2 adsorption–desorpotion isotherms and pore size distribution [inset] of HZSM–5 synthesized using trimethoxymethylsilane (MTS), trimethoxy(propyl)silane (PTS), trimethoxy(octyl)silane (OTS) and hexadecyltrimethoxysilane (HTS) under pre–crystallizing 12 h.

The physical properties of conventional and hierarchical HZSM–5 are listed in **Table S1**. The surface areas for all the hierarchical ZSM–5 were higher than that of conventional ZSM–5. The ZMTS had the highest surface area of micropores (S_{micro}) of 240.4 m^2/g and lowest surface area mesopores (S_{meso}) of 129.4 m^2/g amount the four catalysts which mainly because that the MTS did not produce any mesopores. The 129.4 m^2/g of S_{meso} may attribute to the mesopores between each ZSM–5 particles. The ZPTS and ZOTS gave the highest S_{meso} further proved that the PTS and OTS produced intercrystal mesopores. Thus, the carbon chain length of the organosilanes had a significant influence on the hierarchical ZSM–5. The PTS and OTS were suitable to produce intercrystal mesoporosity at about 10–20 nm to form hierarchical ZSM–5 while the HTS produced mainly ntracrystal macroporosity and formed the hierarchical nanocrystalline ZSM–5 proved by the TEM.

The acidity of the conventional and hierarchical ZSM–5 samples was studied by NH_3–TPD and the results are shown in **Figure 5**. For all the profiles, normalization processing to 1 g of catalyst is carried out. All the ZSM–5 samples exhibited two peaks at approximately 200 °C and 450 °C, which represented weak and strong acidity, respectively [40]. The peak intensity of ZMTS was almost the same with HZ–Con meaning the similar amount of acidity both for weak and strong acidity was obtained by these two catalysts because that the MTS did not produce intercrystal mesoporosity like PTS and OTS and the intercrystal macroporosity like HTS. While for the ZHTS sample, the peak area was the highest and acid peak increased to a higher temperature, indicating a higher acid amount and strength, respectively. The hierarchical HZSM–5 zeolites synthesized by PTS and OTS exhibited lowest amount of acid sites because of the small nanoparticles and intercrystal mesopores produced which lower the acidity. It was reported that the acid sites located on the external/mesopore surface have a lower acid strength than those inside the micropore system.

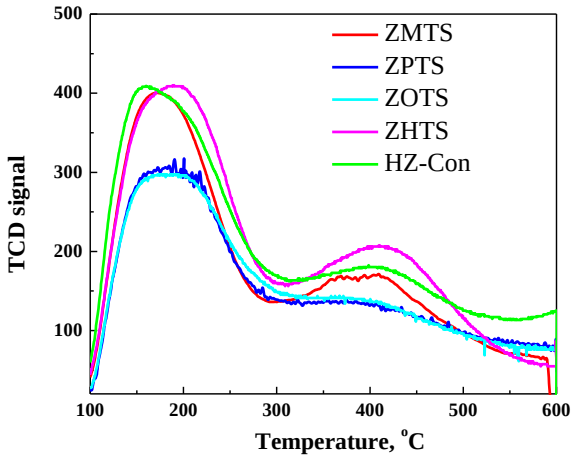

Figure 5. NH_3–TPD patterns of the conventional ZSM–5 and hierarchical ZSM–5 synthesized using trimethoxymethylsilane (MTS), trimethoxy(propyl)silane (PTS), trimethoxy(octyl)silane (OTS) and hexadecyltrimethoxysilane (HTS) under pre–crystallizing 12 h.

CFP of cellulose.

CFP of cellulose was conducted to study the shape–controlled synthesis of hierarchical ZSM–5 with different structures. A control experiment (pyrolysis of cellulose without a catalyst) was conducted, and the products were all oxygenated products without any aromatics. **Figure 6 and Figure 7** show the results of product distribution over conventional and nanocrystalline ZSM–5 synthesized using different organosilanes after pre–crystallizing for

12 h. The product distribution obtained by HZ–Con (33.3% aromatics yield and 36.7% coke yield) was almost the same as for ZMTS (34.4% aromatics yield and 36.1% coke yield). However, the yields of aromatics were different over hierarchical HZSM–5 synthesized by different organosilanes. The aromatics yield decreased for ZPTS (23.1%) and ZOTS (24.8%); and ZHTS showed the highest value for aromatics yield (39.6%) as well as olefins. The yield for coke was in the opposite direction, meaning that the ZSM–5 structure synthesized by HTS not only increased the aromatics yield but also reduced the coke yield. The aromatics distribution as shown in **Figure 6** illustrates that ZHTS also produced the highest yields of BTX (benzene, toluene, and xylene) and heavy aromatics ($C_{10–15}$ aromatics). **Figures S6 and S7** studied the catalytic performance of ZHTS prepared under pre–crystallizing 0 h (ZHTS0), 12 h (ZHTS12) and 24 h (ZHTS24). It was found that the ZHTS12 and ZHTS24 showed higher aromatics yield than the ZHTS0, indicating that the pre–crystallizing played the significant role in the catalysis system. However, there was not any difference between the ZHTS12 and ZHTS24, which showed that the 12 h of pre–crystallizing was enough for the synthesis of ZSM-5.

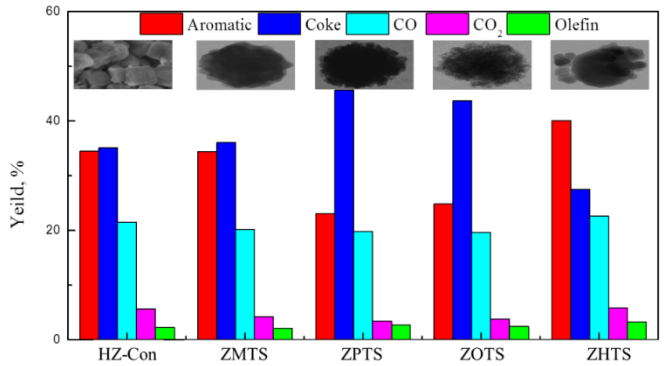

Figure 6. Product distributions in CFP of cellulose over conventional ZSM–5 and hierarchical ZSM–5 synthesized using trimethoxymethylsilane (MTS), trimethoxy(propyl)silane (PTS), trimethoxy(octyl)silane (OTS) and hexadecyltrimethoxysilane (HTS) under pre–crystallizing 12 h. Reaction conditions: 600 °C reaction temperature and 1: 20 biomass/catalyst ratio.

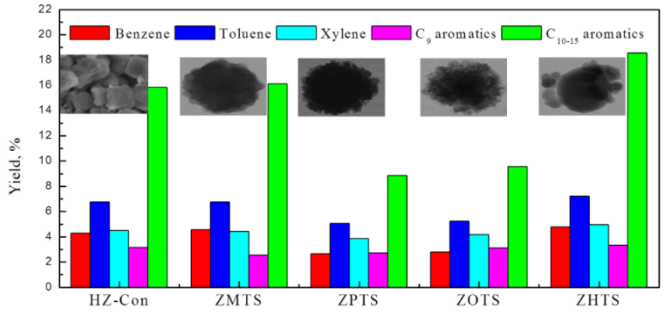

Figure 7. Aromatic distributions in CFP of cellulose over conventional and hierarchical ZSM–5 synthesized using trimethoxymethylsilane (MTS), trimethoxy(propyl)silane (PTS), trimethoxy(octyl)silane (OTS) and hexadecyltrimethoxysilane (HTS) under pre–crystallizing 12 h. Reaction conditions: 600 °C reaction temperature and 1: 20 biomass/catalyst ratio.

Although the hierarchical ZSM-5 was reported to be synthesized by pre–crystallization and applied for the CFP of cellulose[33], the factors influenced the CFP of cellulose were the suitable mesopores and acidity formed by sucrose. This published work emphasized major on the mesopores introduced, which were not controllable because the template was only sucrose[33]. In this work we showed that the morphology of ZSM–5 was controlled by the organosilanes with different carbon chains and significantly influenced the production of aromatics from CFP of cellulose. This controlling the growth of molecular sieve with different functional structures from individual “classic-boat” microporous ZSM-5 to ZSM-5 microspheres with micropores and intercrystal mesopores, and then to the new structure with micropores and intercrystal macropores. The different structure gave different fast catalytic pyrolysis activity, showing the clear structure-property correlation. As shown in **Figure 4**, ZMTS did not show any mesopore size distribution as the HZ–Con. Thus, ZMTS showed a similar structure and catalytic activity to HZ–Con. The yields of total aromatics, BXT, and $C_{10–15}$ aromatics were almost the same. The results of N_2–BET and TEM showed that the shape of ZHTS was some nanocrystalline ZSM–5 particles grafted on the surface of an intact ZSM–5 zeolite. Thus, the ZHTS showed both regular intracrystal microporosity and intercrystal macroporosity. This structure of hierarchical nanocrystalline ZSM–5 had the advantages of microporous and hierarchical structure in ZSM–5, which combined both high relative crystallinity and improved mass transfer by the intercrystal macropores, and benefited the yield of aromatics, especially BXT and yield $C_{10–15}$ aromatics. Conversely, the mesopores in ZPTS and ZOTS were not suitable; and the yields of total aromatics, BXT, and $C_{10–15}$ aromatics were lower than for ZHTS and even for ZMTS and conventional HZSM–5. This new HZSM–5 structure can also reduce coke formation during CFP of cellulose as a result of enhanced mass transfer of moleculars. In conclusion, the synthesized ZSM-5 with the efficient structure in this work showed higher catalytic activity for both increasing aromatics yield and decreasing coke yield (39.6% total aromatics yield and 27.5% coke yield) than that synthesized by hard template using sucrose (37.0% total aromatics yield and 30.5% coke yield)[33].

Acidity was another significant factor. The hierarchical HZSM–5 zeolites synthesized by PTS and OTS exhibited the lowest acidity and gave the lowest total yields of aromatics, BXT, and $C_{10–15}$ aromatics. ZHTS, which had the highest acidity, gave the highest yield of aromatics. We measured the Py-FTIR spectra of ZMTS, ZPTS and ZHTS to study the distribution of Brønsted and Lewis acidity in micropores (pyridine) and mesopores/macropores (dimethyl pyridine) as shown in **Figure S3**. For all the profiles, normalization processing to 1 g of catalyst is carried out. It was found that the ZMTS had a certain amount of Lewis acid site in micropores without any Brønsted acidity. The Brønsted/Lewis distribution was almost the same for the ZPTS and ZMTS. It was interesting to find that the ZHTS not only showed higher amount of Lewis acidity than ZPTS and ZMTS, but also showed a certain amount of Brønsted acidity for both strong and weak acidity. However, for acidity detected by dimethyl pyridine, it was found that no Brønsted/Lewis acidity in mesopores/macropores. This was because the mesopores/macropores were all intercrystal pores. It was reported that the olefins obtained by cracking and dehydrogenation on Brønsted acid sites were converted into cycloalkanes by Diels–Alder cyclization at Lewis acid site, and then

the cycloalkanes were transferred to acid sites to form aromatics by dehydrogenation–aromatization at Brønsted acid sites. [40, 41]. Thus, the higher the acidity of the ZSM–5, the higher the yield of aromatics obtained.

Experimental

Materials and Methods

$NaAlO_2$ (99%), sucrose (AR), tetraethyl orthosilicate (TEOS, >99%), trimethoxymethylsilane (MTS, 98%), trimethoxy(propyl)silane (PTS, 98%), trimethoxy(octyl)silane (OTS, 98%), hexadecyltrimethoxysilane (HTS, 85%) and trimethoxyoctadecylsilane (TTS, 90%) were purchased from Aladdin, Shanghai. Tetrapropylammonium hydroxide (TPAOH, 25wt%) and NH_4Cl (AR) were purchased from Sinopharm Chemical Reagent Co., Ltd. Cellulose (20 μm) was brought from Sigma–Aldrich.

Synthesis of hierarchical ZSM–5

Hierarchical ZSM–5 samples were synthesized by a pre–crystallization process using organosilanes as mesopore templates. The molar compositions of the mixtures were controlled as Al_2O_3: SiO_2: TPAOH: M (M=MTS, PTS, OTS and HTS): H_2O=1.1: 30: 6: 1.5: 750. In a typical synthesis, $NaAlO_2$ and TPAOH were dissolved in H_2O and stirred for 0.5 h. Then, TEOS was added into the resulting solution under vigorous stirring. This aluminosilicate gel was stirred for 3 h at room temperature, and pre–crystalized at 90 °C for 12 h. Then, organosilane (MTS, PTS, OTS and HTS) was added into the gel and stirred at 90 °C for 3 h. The final mixtures were transferred into an autoclave and crystallized at 170 °C for 72 h. The precipitated products were filtered and washed with distilled water. The obtained samples were dried at 110 °C for 12 h and subsequently calcined at 550 °C in air for 6 h (1 °C/min). The resulted samples were converted to the H–form by three consecutive exchanges in 1.0 M NH_4Cl solution at 80 °C for 8 h. After subsequently calcined at 550 °C in air for 6 h (1 °C/min), the samples were denoted ZMTS, ZPTS, OTS and ZHTS, respectively.

ZHTS0, ZHTS12 and ZHTS24 samples were synthesized under the same conditions but altered the pre–crystallization time to 0h, 12 h and 24 h.

Conventional ZSM–5 was synthesized only using TPAOH as the micropore template. The molar compositions of the mixtures were controlled as Al_2O_3: SiO_2: TPAOH: H_2O=1.05: 30: 6: 750 and the ZSM–5 was synthesized under the same conditions showed above. The sample was denoted HZ–Con.

Characterization of the catalysts

The TEM specimen was examined on a Zeiss Libra 120 Plus TEM (Carl Zeiss NTS, Oberkochen, Germany) operating at 120 kV with 20 eV in–column energy filtering. The micrographs were acquired by a Gatan UltraScan 4Kx4K CCD. Four types of samples were ultrasonically dispersed 30 min. An aliquot (~4 μl) of sample was placed on a glow–discharged thin–carbon–coated 200 mesh copper grid (CF200–UL, Electron Microscopy Sciences, Hatfield, PA 19440, USA), then was dried by air.

N_2 adsorption and desorption isotherms were measured on a Micromeritics 3Flex adsorption instrument. The samples were degassed for 12 h under N_2 at 300 °C prior to the measurements. The microporous volume, microporous surface area, and external surface area were calculated by the t–plot method. The mesopore volume and size distribution were obtained from the adsorption branch of the isotherm using the Barrett–Joyner–Halenda (BJH) method.

XRD patterns were recorded on a Shimadzu XRD–6000 diffractometer with Cu–Kα radiation at 40 kV and 40 mA. The diffractions were carried out in the 2θ range of 5~50° at a rate of 4°/min.

NH_3–TPD experiments were measured on a connected thermal conductivity detector (TCD). Typically, 50 mg of the zeolite was pretreated at 500 °C in He (20 mL/min) for 2 h and then cooled to 80 °C before NH_3 adsorption for 40 min. Ammonia desorption measurements were achieved in the temperature range of 80~700 °C at a ramping rate of 10 °C/min.

The distribution of Lewis and Brønsted acids was determined by infrared spectroscopy of adsorbed pyridine (Vertex 70, Bruker). The analysis of Brønsted and Lewis acid sites was carried out using the absorption at 1545 and 1454 cm^{-1}, respectively.

Mercury injection test was used to detect the macrospores.

CFP of cellulose

The CFP of cellulose experiments were conducted in a Tandem μ–reactor system (Rx–3050 TR, Frontier Laboratories, Japan) coupled directly to a GC/MS for identification and quantification of the pyrolysis products. The furnace consisted of two reactors (upper and lower), both of which could be individually temperature–controlled from 40~900 °C. The interface between the furnaces and the GC could be heated to 100~400 °C, which was operated at 300 °C to minimize the condensation of the pyrolysis products. For a typical test of catalytic pyrolysis, approximately 4 mg of a mixture with catalyst/cellulose ratio of 20:1 in mass was added. He was used as the pyrolysis gas and the carrier gas. The reaction temperature was 600 °C.

The pyrolysis vapor was swept into a gas chromatograph (Agilent 7890 B) equipped with a three–way splitter coupled to three detectors: a mass spectrometer (5977A MSD), a flame–ionization detector (FID), and a thermal–conductivity detector (TCD). A liquid nitrogen bath (MicroJet Cryo–Trap, MJT–1030E) was used to focus the pyrolysis vapors of the volatile components, such as CO, CO_2, light olefins and alkanes. A good separation effect for the vapors was achieved by rapidly cooling and concentrating the vapors using liquid nitrogen at the head of the column to increase the peak resolution. The condensable pyrolysis products were separated with an Ultra alloy–5 capillary column (30 m × 0.250 mm and film thickness of 2 μm). The yields of CO and CO_2 were quantified by TCD and the other organic products were quantified by FID by external standard. Yields of product was reported as the molar carbon yield, defined as the molar ratio of carbon in a specific product to the carbon in cellulose. The aromatic selectivity was defined as the ratio of the target aromatic to the total aromatic products. The unaccounted contents were unrecovered coke deposited on the walls of the sample cups. All measurements were repeated three times under the same conditions to check the reproducibility of the data, and average values were calculated for each test.

Conclusions

In conclusion, hierarchical ZSM-5 were synthesized using four different organosilanes (MTS, PTS, OTS, and HTS) as mesoporous templates. The HTS produced hierarchical ZSM-5 in a new structure

with some nanocrystalline ZSM-5 particles on the surface of an intact ZSM-5. This structure with micropores and intercrystal macropores kept both high crystallinity, acidity and mass transfer ability. PTS and OTS produced hierarchical nanocrystalline ZSM-5 with a structure of microspheres aggregated with many nanoscale ZSM-5 particles, and MTS formed the classical one–by–one HZSM-5 morphology with only micropores. The ZSM-5 synthesized by PTS and OTS had weaker acidity than that synthesized by MTS and HTS due to the low crystallinity of ZSM-5 nanosphere and intercrystal mesoporosity. The CFP of cellulose results showed that ZHTS gave the highest total aromatics yield (39.6%) and the lowest coke yield (27.5%) due to the efficient hierarchical ZSM-5 structure.

Conflicts of interest

There are no conflicts to declare.

Acknowledgements

This work was supported by the National Natural Science Foundation of China (No. 21436007, 21676243, 21706228) and the Zhejiang Provincial Natural Science Foundation of China (No. LR17B060002). SD was supported by the Division of Chemical Sciences, Geosciences, and Biosciences, Office of Basic Energy Sciences, U.S. Department of Energy. Work at the Molecular Foundry was supported by the Office of Science, Office of Basic Energy Sciences of the U.S. Department of Energy under Contract No. DE-AC02-05CH11231. J.L. was partially supported by the National Heart, Lung, and Blood Institute of the National Institutes of Health (No. R01HL115153) and the National Institute of General Medical Sciences of the National Institutes of Health (No. R01GM104427).

Notes and references

1 G. W. Huber and A. Corma, *Angew. Chem. Int. Ed.,* 2007, **46**, 7184.
2 A. Corma, S. Iborra and A. Velty, *Chem. Rev.,* 2007, **107**, 2411.
3 G. T. Neumann and J. C. Hicks, *ACS Catal.,* 2012, **2**, 642.
4 K. Wang, J. Zhang, B. H. Shanks and R. C. Brown, *Green Chem.,* 2015, **17**, 557.
5 Y. T. Cheng, Z. Wang, C. J. Gilbert, W. Fan and G. W. Huber, *Angew. Chem. Int. Ed.,* 2012, **51**, 11097.
6 Y. T. Cheng and G. W. Huber, *ACS Catal.,* 2011, **1**, 611.
7 J. N. Chheda, G. W. Huber and J. A. Dumesic, *Angew. Chem. Int. Ed.,* 2007, **46**, 7164.
8 J. Liang, Z. Liang, R. Zou and Y. Zhao, *Adv. Mater.,* 2017. **29**, 1701139.
9 D. Nandan, S. K. Saxena and N. Viswanadham, J. Mater. Chem. A, 2014, 2, 1054-1059.
10 D. Wang, L. Xu and P. Wu, J. Mater. Chem. A, 2014, 2, 15535-15545.
11 G. Feng, P. Cheng, W. Yan, M. Boronat, X. Li, J. Su, J. Wang, Y. Li, A. Corma, R. Xu and J. Yu, *Science*, 2016, **351,** 1188.
12 K. Na, C. Jo, J. Kim, K. Cho, J. Jung, Y. Seo, R. J. Messinger, B. F. Chmelka and R. Ryoo, *Science*, 2011, **333**, 328.
13 E. Mahmoud, J. Yu, R. J. Gorte and R. F. Lobo, *ACS Catal.*, 2015, **5**, 6946.
14 C. M. Parlett, K. Wilson and A. F. Lee, *Chem. Soc. Rev.*, 2013, **42**, 3876.
15 D. P. Serrano, J. M. Escola and P. Pizarro, *Chem. Soc. Rev.,* 2013, **42**, 4004.
16 Y. Tao, H. Kanoh, L. Abrams and K. Kaneko, *Chem. Rev.,* 2006, **106**, 896.
17 D. Gao, A. Zheng, X. Zhang, H. Sun, X. Dai, Y. Yang, H. Wang, Y. Qin, S. Xu and A. Duan, *Nanoscale*, 2015, **7**, 10918-10924.
18 J. Pérez–Ramírez, D. Verboekend, A. Bonilla and S. Abelló, *Adv. Funct. Mater.,* 2009, **19**, 3972.
19 J. C. Groen, T. Sano, J. A. Moulijn and J. Pérez–Ramírez, *J. Catal.,* 2007, **251**, 21.
20 Pérez-Ramírez, S. Abelló, A. Bonilla and J. C. Groen, *Adv. Funct. Mater.,* 2009, **19**, 164.
21 K. Qiao, X. Shi, F. Zhou, H. Chen, J. Fu, H. Ma and H. Huang, *Appl. Catal. A: Gen.*, 2017, **547**, 274.
22 H. Chen, H. Cheng, F. Zhou, K. Chen, K. Qiao, X. Lu, P. Ouyang and J. Fu, *J. Anal. Appl. Pyrol.*, 2018, **131**, 76.
23 J. Li, X. Li, G. Zhou, W. Wang, C. Wang, S. Komarneni and Y. Wang, *Appl. Catal. A: Gen.,* 2014, **470**, 115.
24 B. Li, B. Sun, X. Qian, W. Li, Z. Wu, Z. Sun, M. Qiao, M. Duke and D. Zhao, *J. Am. Chem. Soc.,* 2013, **135**, 1181.
25 W. Fan, M. A. Snyder, S. Kumar, P. S. Lee, W. C. Yoo, A. V. McCormick, R. L. Penn, A. Stein and M. Tsapatsis, *Nat. Mater.,* 2008, **7**, 984.
26 X. Zhang, D. Liu, D. Xu, S. Asahina, K. A. Cychosz, K. V. Agrawal, Y. Al Wahedi, A. Bhan, S. Al Hashimi, O. Terasaki, M. Thommes and M. Tsapatsis, *Science,* 2012, **336**, 1684.
27 D. W. Fickel, E. D'Addio, J. A. Lauterbach and R. F. Lobo, *Appl. Catal. B: Environ.,* 2011, **102**, 441.
28 M. Choi, K. Na, J. Kim, Y. Sakamoto, O. Terasaki and R. Ryoo, *Nature,* 2009, **461**, 246.
29 M. Choi, H. S. Cho, R. Srivastava, C. Venkatesan, D. H. Choi and R Ryoo, *Nat. Mater.,* 2006, **5**, 718.
30 X. Qian, J. Du, B. Li, M. Si, Y. Yang, Y. Hu, G. Niu, Y. Zhang, H. Xu, B. Tu, Y. Tang and D. Zhao, *Chem. Sci.,* 2011, **2**, 2006.
31 Z. Xue, J. Ma, T. Zhang, H. Miao and R. Li, *Mater. Lett.,* 2012, **68**, 1.
32 S. Ivanova, B. Louis, M. J. Ledoux and C. Pham-Huu, *J. Am. Chem. Soc.,* 2007, **129**, 3383.
33 H. Chen, X. Shi, F. Zhou, H. Ma, K. Qiao, X. Lu, J. Fu and H. Huang, *Catal. Commun.*, 2018, **110**, 102.
34 H. Chen, Q. Wang, X. Zhang and L. Wang, *Ind. Eng. Chem. Res.,* 2014, **53**, 19916.
35 J. A. Botas, D. P. Serrano, A. García and R. Ramos, Appl. Catal. B: *Environ.,* 2014, **145**, 205.
36 D. P. Serrano, J. Aguado, J. M. Escola, J. M. Rodríguez and Á. Peral, Chem. Mater. 2006, 18, 2462.
37 D. P. Serrano, J. Aguado, J. M. Escola, J. M. Rodriguez and Á. Peral, J. Mater. Chem. 2008, 18, 4210.
38 H. Chen, X. Zhang, J. Zhang and Q. Wang, RSC Adv. 2017, 7, 46109.
39 A. I. Lupulescu and J. D. Rimer, Science 2014, 344, 729.
40 A. G. Gayubo, A. T. Aguayo, A. Atutxa, R. Aguado and J. Bilbao, Ind. Eng. Chem. Res. 2004, 43, 2610.
41 H. Chen, Q. Wang, X. Zhang and L. Wang, *Appl. Catal. B: Environ.*, 2015, **166-167**, 327.

TOC:

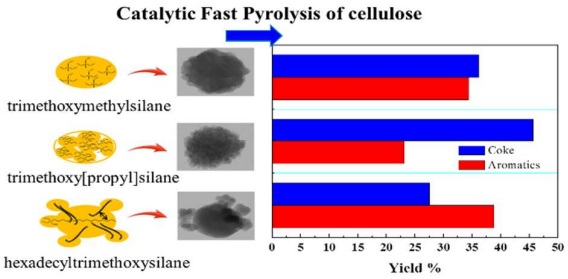
Catalytic Fast Pyrolysis of cellulose
trimethoxymethylsilane
trimethoxy[propyl]silane
hexadecyltrimethoxysilane
Coke
Aromatics
0 5 10 15 20 25 30 35 40 45 50
Yield %